

Journal of
Mechanics of
Materials and Structures

**AN ASYMPTOTIC ANALYSIS OF ANISOTROPIC
HETEROGENEOUS PLATES WITH CONSIDERATION OF END
EFFECTS**

Jun-Sik Kim

Volume 4, N^o 9

November 2009

 mathematical sciences publishers

AN ASYMPTOTIC ANALYSIS OF ANISOTROPIC HETEROGENEOUS PLATES WITH CONSIDERATION OF END EFFECTS

JUN-SIK KIM

A finite element-based asymptotic analysis tool is developed for general anisotropic plates. The formulation begins with three-dimensional equilibrium equations in which the thickness coordinate is scaled by the characteristic length of the plate. This allows us to split the equations into two parts, such as the one-dimensional microscopic equations and the two-dimensional macroscopic equations, via the virtual work concept. The one-dimensional microscopic analysis yields the through-the-thickness warping function at each level, which does not require two-dimensional macroscopic analysis. The two-dimensional macroscopic equations provide the governing equations of the plate at each level in a recursive form. These can be solved in an orderly manner, in which proper macroscopic boundary conditions should be incorporated. The displacement prescribed boundary condition is obtained by introducing the orthogonality condition of asymptotic displacements to the plate fundamental solutions. In this way, the end effects of the plate are kinematically corrected without applying the sophisticated decay analysis method. The developed asymptotic analysis method is applied to semiinfinite plates with simply supported and clamped-free boundary conditions. The results obtained are compared to those of three-dimensional FEM, three-dimensional elasticity, and Reissner–Mindlin plate theory. The usefulness of the present method is also discussed.

1. Introduction

Analysis of anisotropic plates has been extensively carried out since the Kirchhoff–Love and Reissner–Mindlin plate theories were developed. It has been a challenging class of problems, involving the prediction of the behavior of anisotropic elastic bodies, including plates made of emerging composite materials, with sufficient accuracy while maintaining a low number of degrees of freedom. Accordingly many higher-order plate theories have been developed beyond the classical Kirchhoff–Love and Reissner–Mindlin plate theories. One can categorize them into three classes: smeared theories, zig-zag theories, and layerwise theories. Comprehensive reviews and assessments can be found in the surveys [Kapania and Raciti 1989; Noor and Burton 1989; Reddy and Jr. 1994; Carrera 2003].

Most theories reported in the literature are based on an a priori kinematic assumption which describes the higher-order behavior of plates especially for transverse shear deformation. This kinematic assumption leads to the improved prediction of transverse shear stresses that is crucial for stress analysis of laminated composite plates. Some of the higher-order theories are quite successful at describing such composite plates by increasing the number of degrees of freedom. For example, the higher-order theory developed by Lo et al. [1977] provides the accurate through-the-thickness distribution of transverse shear stresses for the plates made of isotropic materials. However the accuracy of this theory is degraded when

Keywords: composite plate, sandwich plate, formal asymptotic method, end effect, boundary condition, FAMPA.

a plate made of highly anisotropic materials is considered, especially one weak in shear. This triggered the development of various higher order plate theories in the last two decades.

One of the major drawbacks of these higher-order theories is that we do not know how accurate they are. These theories strongly depend on a priori assumed warping functions that are generally functions of the material properties and loading conditions. Thus it is crucial to find and/or assume the proper warping functions and desirable to obtain these from the three-dimensional (3D) elasticity if possible. One can derive them from the 3D elasticity by applying asymptotic methods which are mathematically rigorous. There are three types of asymptotic methods: the formal asymptotic method [Niordson 1979], the variational-asymptotic method (VAM) [Berdichevskii 1979; Berg 1991], and the asymptotic integration method [Novotny 1970; Wang and Tarn 1994; Tarn et al. 1996]. There is however a critical bottleneck associated with these asymptotic methods, and that is a proper set of boundary conditions. It is not trivial to exactly satisfy 3D boundary conditions especially for a displacement prescribed boundary condition [Duva and Simmonds 1992]. One can obtain asymptotically correct boundary conditions without solving the boundary layer problems by applying the decay analysis method [Gregory and Wan 1984]. Fan and Widera [1994] demonstrated that the displacement prescribed boundary conditions obtained via this method are different from those derived by variational principles. It is however too difficult to obtain these boundary conditions via the decay analysis method for engineering applications. For this very reason, an asymptotic analysis is often limited to the classical approximation for clamped plates and plates with simply supported boundary conditions. Another way to avoid the problem associated with boundary conditions is to derive a Reissner–Mindlin-like (RM-like) plate theory. Recently, Yu et al. [2002] and Yu [2005] have developed the RM-like plate models by applying the VAM and using the through-the-thickness finite element analysis. These models are not claimed to be asymptotically correct. And the asymptotically correct solutions up to $\mathcal{O}(\epsilon^2)$, which are comparable to those of the Reissner–Mindlin theory, have not been known for general anisotropic heterogeneous plates with clamped boundaries.

In this paper, a formal asymptotic expansion method is employed to derive a set of recursive equilibrium equations and boundary conditions from the 3D linear elasticity. We first split the 3D equilibrium equations into two sets of one-dimensional (1D) microscopic and two-dimensional (2D) macroscopic problems by introducing the virtual work concept. A conventional finite element discretization is then applied to solve the problems. The 1D microscopic analysis, which is the through-the-thickness analysis, yields the warping functions corresponding to the classical strain measure at each level. These functions are smeared into the stiffness models used for the 2D macroscopic formulation. Once the microscopic and macroscopic equations are derived, one has to determine a proper set of boundary conditions. We recast the strong forms of the equilibrium equations obtained in their corresponding weak forms. During this process, the displacement boundary conditions are treated as constraints in the weak form. In this way, the asymptotic displacement can be correlated to the boundary condition, and the asymptotically correct boundary condition up to $\mathcal{O}(\epsilon^2)$ can be derived. Thus one can obtain the asymptotically correct solution immediately next to the classical solution for general boundary conditions.

The results obtained are compared to those of the 3D FEM, 3D elasticity, and RM plate theory. Through numerical examples, this paper demonstrates how the edge zone affects the interior solution via a proper set of boundary conditions. This defines the term “end effects” used in this paper. The microscopic solutions, which can be obtained without solving the macroscopic problems, are also discussed to convey the usefulness of the proposed approach.

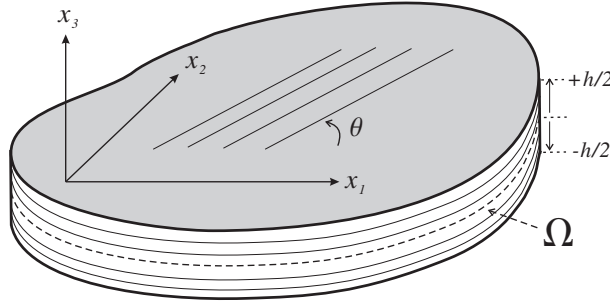


Figure 1. Geometry and coordinates of laminated plates.

2. Formal asymptotic formulation

A 3D composite plate with material anisotropy is considered in this study (see Figure 1). In order to apply the asymptotic expansion method, one needs to define a small parameter (ϵ) in terms of the thickness dimension which is much less than the in-plane dimension. To this end, the coordinates are scaled as

$$y_\alpha = x_\alpha, \quad y_3 = \frac{x_3}{\epsilon}, \tag{1}$$

in which ϵ is defined to be $\epsilon = h/l_c$, where h and l_c represent the thickness and characteristic length of the plate, respectively.

2.1. 3D equilibrium equations and boundary conditions. In the scaled coordinates from (1), the 3D static problem of linear elasticity, which consists of equilibrium equations, strain-displacement relationships, and constitutive equations, can be expressed as

$$\begin{aligned} \sigma_{ij,j} + \tilde{b}_i &= 0 & \rightarrow & \quad \frac{1}{\epsilon} \mathcal{L}_3^t \sigma_{,3} + \mathcal{L}_\alpha^t \sigma_{,\alpha} + \tilde{\mathbf{b}} = 0, \\ \epsilon_{ij} &= \frac{1}{2} (u_{i,j} + u_{j,i}) & \rightarrow & \quad \boldsymbol{\epsilon} = \frac{1}{\epsilon} \mathcal{L}_3 \mathbf{u}_{,3} + \mathcal{L}_\alpha \mathbf{u}_{,\alpha}, \\ \sigma_{ij} &= c_{ijkl} \epsilon_{kl} & \rightarrow & \quad \boldsymbol{\sigma} = \frac{1}{\epsilon} \mathbf{C} \mathcal{L}_3 \mathbf{u}_{,3} + \mathbf{C} \mathcal{L}_\alpha \mathbf{u}_{,\alpha}, \end{aligned} \tag{2}$$

where a subscript $(\cdot)_{,i}$ indicates the partial derivative with respect to the coordinate y_i , a superscript t denotes the transpose of a matrix or vector, c_{ijkl} represent components of the 3D elasticity tensor, a body force vector $\tilde{\mathbf{b}}$, and a displacement vector \mathbf{u} . Stress and strain tensors are expressed in the vector form

$$\boldsymbol{\epsilon} = [\epsilon_{11} \ \epsilon_{22} \ \epsilon_{33} \ 2\epsilon_{23} \ 2\epsilon_{13} \ 2\epsilon_{12}]^t, \quad \boldsymbol{\sigma} = [\sigma_{11} \ \sigma_{22} \ \sigma_{33} \ \sigma_{23} \ \sigma_{13} \ \sigma_{12}]^t. \tag{3}$$

The linear operators \mathcal{L}_i are defined by

$$\mathcal{L}_1 = \begin{bmatrix} 1 & 0 & 0 \\ 0 & 0 & 0 \\ 0 & 0 & 0 \\ 0 & 0 & 0 \\ 0 & 0 & 1 \\ 0 & 1 & 0 \end{bmatrix}, \quad \mathcal{L}_2 = \begin{bmatrix} 0 & 0 & 0 \\ 0 & 1 & 0 \\ 0 & 0 & 0 \\ 0 & 0 & 1 \\ 0 & 0 & 0 \\ 1 & 0 & 0 \end{bmatrix}, \quad \mathcal{L}_3 = \begin{bmatrix} 0 & 0 & 0 \\ 0 & 0 & 0 \\ 0 & 0 & 1 \\ 0 & 1 & 0 \\ 1 & 0 & 0 \\ 0 & 0 & 0 \end{bmatrix}. \tag{4}$$

The boundary conditions considered herein are summarized as

$$\mathbf{u} = \bar{\mathbf{u}} \text{ on } S_u, \quad \boldsymbol{\sigma} \boldsymbol{\nu} = \tilde{\mathbf{p}} \text{ on } S_\sigma, \quad \boldsymbol{\sigma} \boldsymbol{\nu} = \tilde{\mathbf{g}} \text{ on } \Omega^\pm, \tag{5}$$

where S_u and S_σ represent the edge boundaries with prescribed displacements $\bar{\mathbf{u}}(x_i)$ and prescribed traction $\tilde{\mathbf{p}}(x_i)$, respectively. Ω^\pm denotes the top and bottom surfaces of the plate, and $\boldsymbol{\nu}$ is the direction cosine of the outward normal to the boundaries S_σ and Ω^\pm .

2.2. Asymptotic expansion and scaling. The displacement is expanded in terms of the small parameter

$$\mathbf{u} = \mathbf{u}^{(0)} + \epsilon \mathbf{u}^{(1)} + \epsilon^2 \mathbf{u}^{(2)} + \epsilon^3 \mathbf{u}^{(3)} + \dots, \tag{6}$$

where the 0th order displacement needs special attention, because it is related to the asymptotic convergence [Buannic and Cartraud 2001; Kim et al. 2008]. Each order displacement is given by

$$\mathbf{u}^{(0)}(y_\alpha) = [0 \ 0 \ u_3^{(0)}]^t, \quad \mathbf{u}^{(k)}(y_i) = [u_1^{(k)} \ u_2^{(k)} \ u_3^{(k)}]^t, \quad k \geq 1, \tag{7}$$

where $u_3^{(0)}(y_i) \equiv v_3^{(0)}(y_\alpha)$. The variables v_i represent functions of the in-plane coordinates y_α only.

The components of body force and surface traction, which are regarded as prescribed quantities, are also scaled as follows:

$$\tilde{b}_\alpha = \epsilon b_\alpha, \quad \tilde{b}_3 = \epsilon^2 b_3, \quad \tilde{p}_\alpha = \epsilon p_\alpha, \quad \tilde{p}_3 = \epsilon^2 p_3, \quad \tilde{g}_\alpha = \epsilon^2 g_\alpha, \quad \tilde{g}_3 = \epsilon^3 g_3, \tag{8}$$

and the prescribed displacement is presupposed by

$$\bar{u}_3 \sim \mathcal{O}(1), \quad \bar{u}_\alpha \sim \mathcal{O}(\epsilon). \tag{9}$$

Substituting (6) and (8) into (2) yields the recursive forms

$$\mathcal{L}_3^t \boldsymbol{\sigma}_{,3}^{(k+1)} = -\mathcal{L}_\alpha^t \boldsymbol{\sigma}_{,\alpha}^{(k)} - \mathbf{b}^{(k)}, \quad \boldsymbol{\epsilon}^{(k+1)} = \mathcal{L}_3 \mathbf{u}_{,3}^{(k+2)} + \mathcal{L}_\alpha \mathbf{u}_{,\alpha}^{(k+1)}, \quad \boldsymbol{\sigma}^{(k+1)} = \mathbf{C} \boldsymbol{\epsilon}^{(k+1)}, \quad k \geq -1, \tag{10}$$

where $\boldsymbol{\sigma}^{(k+1)}$ and $\boldsymbol{\epsilon}^{(k+1)}$ are expanded based on the displacement expansions, (6), and the coordinate scale, (1).

The associated boundary conditions at the edge boundaries are

$$\mathbf{u}^{(k+1)} = \bar{\mathbf{u}}^{(k+1)} \text{ on } S_u, \quad \boldsymbol{\sigma}^{(k+1)} \boldsymbol{\nu} = \mathbf{p}^{(k+1)} \text{ on } S_\sigma, \tag{11}$$

and at the top and bottom surfaces of the plate

$$\boldsymbol{\sigma}^{(k+1)} \boldsymbol{\nu} = \mathbf{g}^{(k+1)} \text{ on } \Omega^\pm, \tag{12}$$

where $\bar{\mathbf{u}}^{(k)} = \mathbf{0}$ if $k \neq 0$ or 1 , $\mathbf{b}^{(k)} = \mathbf{0}$ and $\mathbf{p}^{(k)} = \mathbf{0}$ if $k \neq 1$ or 2 , and $\mathbf{g}^{(k)} = \mathbf{0}$ if $k \neq 2$ or 3 . Notice here that the negative powers of the quantities vanish.

2.3. Fundamental solution. The very first equation ($k = -1$) from (10) can be obtained as

$$\mathcal{L}_3^t \boldsymbol{\sigma}_{,3}^{(0)} = \mathbf{0}. \tag{13}$$

Its solution can be easily found by $\boldsymbol{\sigma}^{(0)} = \boldsymbol{\epsilon}^{(0)} = \mathbf{0}$ since it is well posed [Buannic and Cartraud 2001; Kim et al. 2008]. From $\boldsymbol{\epsilon}^{(0)} = \mathbf{0}$ the particular solution is obtained by

$$\mathbf{u}_p^{(1)} = [-y_3 v_{3,1}^{(0)} \ -y_3 v_{3,2}^{(0)} \ 0]^t. \tag{14}$$

The solution is defined up to a rigid body displacement ($\mathbf{u}_R = \{v_1, v_2, v_3\}$). This forms the fundamental solutions such that

$$\mathbf{u}^{(1)} = \tilde{\mathbf{u}}^{(1)} \equiv \mathbf{u}_p^{(1)} + \mathbf{u}_R^{(1)} = \Theta(y_3)\tilde{\mathbf{v}}^{(1)}(y_\alpha), \quad (15)$$

where

$$\Theta(y_3) = \begin{bmatrix} 1 & 0 & 0 & -y_3 & 0 \\ 0 & 1 & 0 & 0 & -y_3 \\ 0 & 0 & 1 & 0 & 0 \end{bmatrix}, \quad \tilde{\mathbf{v}}^{(1)}(y_\alpha) = \begin{Bmatrix} v_i^{(1)} \\ v_{3,\alpha}^{(0)} \end{Bmatrix}. \quad (16)$$

This fundamental solution appears repeatedly in each order problem.

2.4. Virtual displacement concept to recursive equations. It is more convenient to rewrite the recursive equilibrium equation, (10), in terms of virtual displacements in order to find the solutions of microscopic and macroscopic problems as well as to handle the surface traction on Ω^\pm . To this end, one can multiply by the virtual displacement $\delta\mathbf{u}^{(k+2)t}$ in (10) and (12). By applying integration by parts for the y_3 coordinate, it takes the form

$$\int_\Omega \left[\int_{h_\epsilon} \delta\mathbf{u}_{,3}^{(k+2)t} \mathcal{L}_3^t \boldsymbol{\sigma}^{(k+1)} dy_3 - \int_{h_\epsilon} \delta\mathbf{u}^{(k+2)t} \mathcal{L}_\alpha^t \boldsymbol{\sigma}_{,\alpha}^{(k)} dy_3 - \int_{h_\epsilon} \delta\mathbf{u}^{(k+2)t} \mathbf{b}^{(k)} dy_3 - \delta\mathbf{u}^{(k+2)t} \mathbf{g}^{(k+1)} \Big|_{y_3=\Omega^\pm} \right] d\Omega = 0, \quad (17)$$

where h_ϵ denotes the scaled thickness of a plate. The edge boundary conditions on S_u and S_σ will be considered and discussed in Section 4.

Furthermore the asymptotic displacement $\mathbf{u}^{(k)}$ can be decomposed into two terms such that

$$\mathbf{u}^{(k)}(y_i) = \tilde{\mathbf{u}}^{(k)}(y_i) + \mathbf{u}_w^{(k)}(y_i), \quad k \geq 2, \quad (18)$$

where the first term is the fundamental solution and the second the warping solution. By substituting this into (17), one can obtain two equations corresponding to $\delta\tilde{\mathbf{u}}^{(k+2)}$ and $\delta\mathbf{u}_w^{(k+2)}$. They are referred to as the *macroscopic* problem (or the plate analysis) and the *microscopic* problem (or the through-the-thickness analysis), respectively.

3. Microscopic and macroscopic problems

In this section, we seek the solutions of the microscopic problems and the macroscopic 2D plate equations from (17). The through-the-thickness 1D finite analysis for the microscopic problems is described first. Then the macroscopic 2D plate equilibrium equations, which are built upon the results of microscopic analysis, are derived.

3.1. Microscopic problems. The microscopic problems can be obtained from (17) by collecting the terms associated with the virtual displacement form of the warping solution, $\delta\mathbf{u}_w^{(k)}$. These can be solved by applying the through-the-thickness 1D finite element discretization. Subsequently the warping solution is generalized for each level of the problems.

The second microscopic problem and finite element discretization. The first nontrivial microscopic problem ($k = 0$), which is associated with $\delta \mathbf{u}_w^{(2)}$ in (17), is given by

$$\int_{h_\epsilon} \delta (\mathcal{L}_3 \mathbf{u}_{w,3}^{(2)})^t \mathbf{C} (\Phi \mathbf{e}^{(1)} + \mathcal{L}_3 \mathbf{u}_{w,3}^{(2)}) dy_3 = 0, \tag{19}$$

where

$$\Phi(y_3) = \begin{bmatrix} 1 & 0 & 0 & -y_3 & 0 & 0 \\ 0 & 1 & 0 & 0 & -y_3 & 0 \\ 0 & 0 & 0 & 0 & 0 & 0 \\ 0 & 0 & 0 & 0 & 0 & 0 \\ 0 & 0 & 0 & 0 & 0 & 0 \\ 0 & 0 & 1 & 0 & 0 & -y_3 \end{bmatrix}, \quad \mathbf{e}^{(1)} = [v_{1,1}^{(1)} \quad v_{2,2}^{(1)} \quad v_{1,2}^{(1)} + v_{2,1}^{(1)} \quad v_{3,11}^{(0)} \quad v_{3,22}^{(0)} \quad 2v_{3,12}^{(0)}]^t. \tag{20}$$

In order to solve (19), the finite element discretization is employed by using the standard 1D Lagrangian interpolation function. The warping solution is then expressed by

$$\mathbf{u}_w(y_i) = \mathbf{N}_u(y_3) \bar{\mathbf{u}}_w(y_\alpha), \tag{21}$$

where \mathbf{N}_u is the shape function matrix and $\bar{\mathbf{u}}_w$ is the nodal vector. Plugging (21) into (19) yields

$$\mathbf{K} \bar{\mathbf{u}}_w^{(2)} + \mathbf{F}_{3E} \mathbf{e}^{(1)} = \mathbf{0}, \tag{22}$$

where

$$\mathbf{K} \equiv \langle B_3^t \quad \mathbf{C} \quad B_3 \rangle, \quad \mathbf{F}_{3E} \equiv \langle B_3^t \quad \mathbf{C} \quad \Phi \rangle, \quad B_3 \equiv \mathcal{L}_3 \mathbf{N}_{u,3}, \tag{23}$$

in which

$$\langle \bullet \rangle = \int_{h_\epsilon} \bullet dy_3. \tag{24}$$

One can solve (22) by applying the orthogonality condition to a rigid body displacement [Cesnik et al. 1996; Kim et al. 2008]. Consequently its solution is represented by

$$\bar{\mathbf{u}}_w^{(2)} = \Gamma^{(1)} \mathbf{e}^{(1)}, \quad \Gamma^{(1)} \equiv \mathbf{K}_I \mathbf{F}_{3E}, \tag{25}$$

where the matrix \mathbf{K}_I is related to the inverse matrix of \mathbf{K} and the orthogonality condition to a rigid body displacement [Kim et al. 2008]. Note that each column of $\Gamma^{(1)}$ represents the warping distribution through the thickness of a plate, which corresponds to six warping functions due to two in-plane extensions, one in-plane shear, two bending curvatures, and one twisting curvature. These functions explain the 3D Poisson effect.

The third and higher microscopic problems. The third microscopic problem ($k = 1$) from (17) can be summarized as follows:

$$\int_{h_\epsilon} \delta \mathbf{u}_{w,3}^{(3)t} \mathcal{L}_3^t \boldsymbol{\sigma}^{(2)} dy_3 = \int_{h_\epsilon} \delta \mathbf{u}_w^{(3)t} \mathcal{L}_\alpha^t \boldsymbol{\sigma}_{,\alpha}^{(1)} dy_3 + \int_{h_\epsilon} \delta \mathbf{u}_w^{(3)t} \mathbf{b}^{(1)} dy_3 + \delta \mathbf{u}_w^{(3)t} \mathbf{g}^{(2)} \Big|_{y_3=\Omega^\pm}, \tag{26}$$

where the last term represents the prescribed surface shear traction on Ω^\pm , which is explicitly expressed by

$$\sigma_{\alpha 3}^{(2)\pm} = g_\alpha^\pm \text{ at } y_3 = \pm \frac{h_\epsilon}{2}. \tag{27}$$

After applying the finite element discretization and carrying out tedious but straightforward manipulation, one can obtain

$$\mathbf{K}\bar{\mathbf{u}}_w^{(3)} = -\mathbf{F}_{3E}\mathbf{e}^{(2)} + [V_\alpha + (W_\alpha - W_\alpha^t) \Gamma^{(1)}] \mathbf{e}_{,\alpha}^{(1)} + \mathbf{F}_g^{(2)} + \mathbf{F}_b^{(1)}, \quad (28)$$

where

$$V_\alpha \equiv \langle B_\alpha^t \mathbf{C} \Phi \rangle, \quad W_\alpha \equiv \langle B_\alpha^t \mathbf{C} B_3 \rangle, \quad B_\alpha \equiv \mathcal{L}_\alpha \mathbf{N}_u, \quad (29)$$

and the last two terms on the right side are force vectors that represent the prescribed traction and the body force, respectively. Once we solve (28), the warping solution has the form

$$\bar{\mathbf{u}}_w^{(3)} = \Gamma^{(1)} \mathbf{e}^{(2)} + \Gamma_\alpha^{(2)} \mathbf{e}_{,\alpha}^{(1)} + \bar{\mathbf{u}}_f^{(3)}, \quad (30)$$

where

$$\Gamma_\alpha^{(2)} \equiv \mathbf{K}_I [V_\alpha + (W_\alpha - W_\alpha^t) \Gamma^{(1)}], \quad \bar{\mathbf{u}}_f^{(3)} \equiv \mathbf{K}_I (\mathbf{F}_g^{(2)} + \mathbf{F}_b^{(1)}). \quad (31)$$

By following the same procedure described in the previous microscopic problems, the solution of the fourth microscopic problem ($k = 2$) can be obtained by

$$\bar{\mathbf{u}}_w^{(4)} = \Gamma^{(1)} \mathbf{e}^{(3)} + \Gamma_\alpha^{(2)} \mathbf{e}_{,\alpha}^{(2)} + \Gamma_{\alpha\beta}^{(3)} \mathbf{e}_{,\beta\alpha}^{(1)} + \bar{\mathbf{u}}_f^{(4)}, \quad (32)$$

where

$$\begin{aligned} \Gamma_{\alpha\beta}^{(3)} &\equiv \mathbf{K}_I [W_{\alpha\beta} \Gamma^{(1)} + (W_\alpha - W_\alpha^t) \Gamma_\beta^{(2)}], & W_{\alpha\beta} &\equiv \langle B_\alpha^t \mathbf{C} B_\beta \rangle, \\ \bar{\mathbf{u}}_f^{(4)} &\equiv \mathbf{K}_I [(W_\alpha - W_\alpha^t) \bar{\mathbf{u}}_{f,\alpha}^{(3)} + \mathbf{F}_g^{(3)} + \mathbf{F}_b^{(2)}]. \end{aligned} \quad (33)$$

Similarly, the solutions of the higher than fourth microscopic problems can be now generalized as follows:

$$\bar{\mathbf{u}}_w^{(k)} = \Gamma^{(1)} \mathbf{e}^{(k-1)} + \Gamma_\alpha^{(2)} \mathbf{e}_{,\alpha}^{(k-2)} + \dots + \Gamma_{\alpha\beta\dots\psi}^{(k-2)} \mathbf{e}_{,\psi\dots\beta\alpha}^{(2)} + \Gamma_{\alpha\beta\dots\psi\omega}^{(k-1)} \mathbf{e}_{,\omega\psi\dots\beta\alpha}^{(1)} + \bar{\mathbf{u}}_f^{(k)}, \quad (34)$$

where $k \geq 5$, and

$$\bar{\mathbf{u}}_f^{(m+1)} \equiv \mathbf{K}_I [W_{\alpha\beta} \bar{\mathbf{u}}_{f,\beta\alpha}^{(m-1)} + (W_\alpha - W_\alpha^t) \bar{\mathbf{u}}_{f,\alpha}^{(m)}], \quad (35)$$

$$\Gamma_{\alpha\beta\gamma\dots\psi\omega}^{(m)} \equiv \mathbf{K}_I [W_{\alpha\beta} \Gamma_{\gamma\dots\psi\omega}^{(m-2)} + (W_\alpha - W_\alpha^t) \Gamma_{\omega\psi\dots\gamma\beta}^{(m-1)}], \quad (36)$$

in which $m \geq 4$.

3.2. Macroscopic problems. One can also derive the macroscopic 2D equilibrium equations from (17) by collecting the terms associated with $\delta\bar{\mathbf{u}}^{(k)}$. In this subsection, the equations at each level are derived and the macroscopic 2D constitutive equations are set up, in which the warping solutions obtained in Section 2 are smeared into the macroscopic 2D stiffness.

Equilibrium equations. From (17), the k -th macroscopic problem that is associated with $\delta\bar{\mathbf{u}}^{(k+2)}$ can be summarized as follows:

$$\begin{aligned} \delta v_\alpha^{(k+2)} : & \quad N_{\alpha\beta,\beta}^{(k)} + n_\alpha^{(k)} = 0, \\ \delta v_{3,\alpha}^{(k+1)} : & \quad M_{\alpha\beta,\beta}^{(k)} + Q_\alpha^{(k+1)} - m_\alpha^{(k)} = 0, \quad k \geq 0, \\ \delta v_3^{(k+2)} : & \quad Q_{\alpha,\alpha}^{(k)} + q^{(k)} = 0, \end{aligned} \quad (37)$$

where

$$N_{\alpha\beta}^{(k)} \equiv \langle \sigma_{\alpha\beta}^{(k)} \rangle, \quad M_{\alpha\beta}^{(k)} \equiv \langle -y_3 \sigma_{\alpha\beta}^{(k)} \rangle, \quad Q_\alpha^{(k)} \equiv \langle \sigma_{\alpha 3}^{(k)} \rangle, \quad (38)$$

and the other terms are the contributions of the body force and prescribed traction, which are

$$\begin{aligned} n_\alpha^{(k)} &\equiv \{ \langle b_\alpha \rangle + g_\alpha^+ + g_\alpha^- \} \delta(k-1), \\ m_\alpha^{(k)} &\equiv \left\{ \langle y_3 b_\alpha \rangle + \frac{h_\epsilon}{2} (g_\alpha^+ - g_\alpha^-) \right\} \delta(k-1), \\ q^{(k)} &\equiv \{ \langle b_3 \rangle + g_3^+ + g_3^- \} \delta(k-2), \end{aligned} \quad (39)$$

where $\delta(k-n)$ indicates the Kronecker delta function.

The very first macroscopic problem, which corresponds to $k=0$ in (37), yields the classical assumption of zero shear force such that $Q_\alpha^{(1)}=0$. The second macroscopic problem ($k=1$) forms the classical plate theory, which contains the trivial terms related to the first-order shear forces $Q_\alpha^{(1)}=0$ from the previous macroscopic problem. This problem also includes the second-order shear forces $Q_\alpha^{(2)}$ that are presented in the third macroscopic problem. From these one obtains the first set of equilibrium equations,

$$N_{\alpha\beta,\beta}^{(1)} + n_\alpha^{(1)} = 0, \quad M_{\alpha\beta,\beta\alpha}^{(1)} + m_{\alpha,\alpha}^{(1)} = q^{(2)}. \quad (40)$$

Similarly the second and higher sets of equilibrium equations are now generalized by

$$N_{\alpha\beta,\beta}^{(k)} = 0, \quad M_{\alpha\beta,\beta\alpha}^{(k)} = 0, \quad k \geq 2. \quad (41)$$

It is worth noting that there are no external loadings in the equations with $k \geq 2$ but the solutions of the equations of the preceding level form the fictive volume force acting like the external loading.

Constitutive equations. The k -th order stress resultants ($k \geq 1$) can be defined by

$$\tilde{\mathcal{N}}^{(k)} \equiv \langle \Phi^t \boldsymbol{\sigma}^{(k)} \rangle = \mathcal{A}^{(1)} \mathbf{e}^{(k-1)} + \mathcal{A}_\alpha^{(2)} \mathbf{e}_{,\alpha}^{(k-2)} + \dots + \mathcal{A}_{\alpha\beta\dots\psi\omega}^{(k-1)} \mathbf{e}_{,\omega\psi\dots\beta\alpha}^{(1)} + \tilde{\mathcal{N}}_f^{(k)}, \quad (42)$$

where

$$\tilde{\mathcal{N}}^{(k)} \equiv [N_{11}^{(k)} \quad N_{22}^{(k)} \quad N_{12}^{(k)} \quad M_{11}^{(k)} \quad M_{22}^{(k)} \quad M_{12}^{(k)}]^t, \quad \tilde{\mathcal{N}}_f^{(k)} \equiv V_\alpha^t \bar{\mathbf{u}}_{f,\alpha}^{(k)} + \mathbf{F}_{3E}^t \bar{\mathbf{u}}_f^{(k+1)}, \quad (43)$$

and

$$\begin{aligned} \mathcal{A}^{(1)} &\equiv \langle \Phi^t \mathbf{C} \Phi \rangle + \mathbf{F}_{3E}^t \Gamma^{(1)}, \\ \mathcal{A}_\alpha^{(2)} &\equiv V_\alpha^t \Gamma^{(1)} + \mathbf{F}_{3E}^t \Gamma_\alpha^{(2)}, \\ &\dots \\ \mathcal{A}_{\alpha\beta\dots\omega}^{(n)} &\equiv V_\alpha^t \Gamma_{\beta\dots\omega}^{(n-1)} + \mathbf{F}_{3E}^t \Gamma_{\alpha\beta\dots\omega}^{(n)}, \quad n \geq 3. \end{aligned} \quad (44)$$

The macroscopic constitutive equations include the terms related to the prescribed surface traction on Ω^\pm , $\tilde{\mathcal{N}}_f^{(k)}$, which are not considered in a conventional way to derive the constitutive equations.

4. Weak form of macroscopic 2D equations

A finite element formulation for the macroscopic 2D equilibrium equations presented in Section 3 is described. To this end, we first apply a Galerkin method to the 2D equilibrium equations with edge boundary conditions as constraints, and then transform them to a weak form through integrating by parts

with respect to the in-plane coordinates y_α . This process allows us to have boundary conditions for the problem.

4.1. 2D plate finite element formulation. To convert the sets of macroscopic equilibrium equations in (40) and (41) to the corresponding weak formulations, it is essential to consider the edge boundary conditions given in (11). These edge boundary conditions can be rewritten in the weak forms

$$\int_{S_\sigma} \delta \mathbf{u}^{(k+2)t} (\boldsymbol{\sigma}^{(k+1)} \mathbf{v} - \mathbf{p}^{(k+1)}) dS + \int_{S_u} \delta \mathbf{u}^{(k+2)t} (\boldsymbol{\sigma}^{(k+1)} \mathbf{v} + \boldsymbol{\lambda}^{(k+1)}) dS = 0, \quad (45)$$

which are subject to the constraint

$$\int_{S_u} \delta \boldsymbol{\lambda}^{(k+1)t} (\mathbf{u}^{(k+2)} - \bar{\mathbf{u}}^{(k+2)}) dS = 0, \quad (46)$$

where $k \geq 0$, and $\boldsymbol{\lambda}$ is a Lagrange multiplier which is introduced to enforce the displacement boundary condition on S_u .

The sets of macroscopic equilibrium equations in (40) and (41) can be recast by applying a Galerkin method, where the weighting function is chosen to be a displacement vector such that

$$\mathbf{v}^{(k)} = [v_1^{(k)} \ v_2^{(k)} \ v_3^{(k-1)}]^t, \quad k \geq 1, \quad (47)$$

combining (45). Subsequently integrating by parts yields the following weak formulation for the problem:

$$\int_{\Omega} \left\{ (\delta \mathbf{e}^{(k)})^t \tilde{\mathcal{N}}^{(k)} - (\delta \hat{\mathbf{v}}^{(k)})^t \tilde{\mathcal{B}}^{(k)} \right\} \delta \Omega = (\delta \hat{\mathbf{v}}^{(k)})^t \int_{S_\sigma} \tilde{\mathcal{F}}^{(k)} dS, \quad k \geq 1, \quad (48)$$

where

$$\hat{\mathbf{v}}^{(k)} = [v_\alpha^{(k)} \ v_3^{(k-1)} \ v_{3,\alpha}^{(k-1)}]^t, \quad \tilde{\mathcal{B}}^{(k)} = [n_\alpha^{(k)} \ q^{(k+1)} \ m_\alpha^{(k)}]^t, \quad \tilde{\mathcal{F}}^{(1)} = \Theta^t [p_1 \ p_2 \ p_3]^t, \quad (49)$$

where $\tilde{\mathcal{F}}^{(k)} = 0$ if $k \geq 2$. Notice here that there are remaining boundary conditions associated with $\delta \mathbf{u}_w^{(k+2)}$ which will be discussed in Section 4.2.

Applying a standard finite element discretization procedure to (48) yields the following recursive linear equations:

$$\mathbf{K}_{2D}^{(1)} \hat{\mathbf{V}}^{(k)} = \mathbf{P}_F^{(k)} - \mathbf{P}_N^{(k)} (\mathbf{K}_{2D}^{(n)}, \hat{\mathbf{V}}^{(n)})_{n=2,3,\dots,k}, \quad (50)$$

where $k \geq 1$, $\hat{\mathbf{V}}^{(k)}$ is the k -th order nodal degrees of freedom vector, and $\mathbf{P}_F^{(k)}$ indicates the forcing vector coming from $\tilde{\mathcal{F}}^{(k)}$ and $\tilde{\mathcal{B}}^{(k)}$. The calculation of the 2D stiffness matrices $\mathbf{K}_{2D}^{(k)}$ is associated with the k -th order stress resultant vector $\tilde{\mathcal{N}}^{(k)}$ that includes higher order derivatives with respect to the coordinates y_α . The fictive volume force vector $\mathbf{P}_N^{(k)}$ is computed from the preceding nodal vectors and 2D stiffness matrices. Their explicit forms are omitted for brevity, since they are lengthy but straightforward.

4.2. Boundary conditions. In the process of integrating by parts in Section 4.1, there are remaining boundary conditions associated with $\delta \mathbf{u}_w^{(k+2)}$ and the displacement boundary S_u . These are summarized as follows:

$$\int_{S_\sigma} \delta \mathbf{u}_w^{(k+2)t} (\boldsymbol{\sigma}^{(k+1)} \mathbf{v} - \mathbf{p}^{(k+1)}) dS + \int_{S_u} \delta \mathbf{u}_w^{(k+2)t} (\boldsymbol{\sigma}^{(k+1)} \mathbf{v} + \boldsymbol{\lambda}^{(k+1)}) dS + \int_{S_u} \delta \tilde{\mathbf{u}}^{(k+2)t} \boldsymbol{\lambda}^{(k+1)} dS = 0, \quad (51)$$

with the constraint given in (46). These boundary conditions carry physical significance, which implies that one cannot exactly satisfy the 3D edge boundary conditions even for stress edge data unless the boundary layer problem is solved. The first term, which is the edge traction, is dismissed in the weighted average sense. The second and third terms are also dismissed if one can properly prescribe the fundamental and warping displacements at the edge on S_u .

A clue to this displacement boundary condition can be sought by examining the displacement constraint. From (51), a Lagrange multiplier can be found. Substituting this into the constraint in (46) yields

$$\int_{S_u} \delta(\boldsymbol{\sigma}^{(k+1)} \mathbf{v})^t (\mathbf{u}^{(k+2)} - \bar{\mathbf{u}}^{(k+2)}) dS = 0, \tag{52}$$

which leads to the so-called averaged displacement boundary condition. For example, this can be simplified for the straight edge perpendicular to the y_1 coordinate by

$$\int_{S_u} \delta \sigma_{i1}^{(k+1)} (u_i^{(k+2)} - \bar{u}_i^{(k+2)}) dS = 0. \tag{53}$$

Furthermore if one assumes linear variations of in-plane stresses and a constant transverse shear stress, the stress edge data is expressed by $\sigma_{\alpha 1} = \tau_\alpha + y_3 \omega_\alpha$ and $\sigma_{31} = \tau_3$. Plugging this into (53) yields five equations such that

$$\begin{aligned} \delta \tau_\alpha &: \quad \langle u_\alpha^{(k+2)} - \bar{u}_\alpha^{(k+2)} \rangle = 0, \\ \delta \omega_\alpha &: \quad \langle y_3 (u_\alpha^{(k+2)} - \bar{u}_\alpha^{(k+2)}) \rangle = 0, \\ \delta \tau_3 &: \quad \langle u_3^{(k+2)} - \bar{u}_3^{(k+2)} \rangle = 0, \end{aligned} \tag{54}$$

which in matrix form is

$$\delta \boldsymbol{\tau}^t \langle \boldsymbol{\Theta}^t (\mathbf{u}^{(k+2)} - \bar{\mathbf{u}}^{(k+2)}) \rangle = 0. \tag{55}$$

This actually yields the same form as the orthogonality condition of asymptotic displacements to the fundamental displacement [Kim et al. 2008]. The displacement condition given in (55) was proven to be asymptotically correct up to $\mathcal{O}(\epsilon^2)$ for a transversely isotropic semiinfinite beam [Horgan and Simmonds 1991]. In this way, one can avoid the overwhelming complexity of using the decay analysis method [Gregory and Wan 1984] to find the asymptotically correct boundary conditions up to any desired order. It is however limited to asymptotic analysis up to $\mathcal{O}(\epsilon^2)$ when the displacement prescribed boundary is considered (for example, for clamped boundaries) [Horgan and Simmonds 1991; Duva and Simmonds 1992].

The orthogonality condition of asymptotic displacements [Kim et al. 2008], which generalizes the averaged displacement boundary condition, is given by

$$\int_{S_u} (\delta \tilde{\mathbf{u}}^{(k)})^t (\mathbf{u}^{(k)} - \bar{\mathbf{u}}^{(k)}) dS = 0, \tag{56}$$

in which $\bar{\mathbf{u}}^{(k)}$ is the scaled displacement edge data. Plugging (15) into this yields

$$(\delta \tilde{\mathbf{v}}^{(k)})^t \mathbf{U}^{(k)} = 0, \quad \mathbf{U}^{(k)} \equiv \int_{S_u} \boldsymbol{\Theta}^t (y_3) (\mathbf{u}^{(k)} - \bar{\mathbf{u}}^{(k)}) dS, \tag{57}$$

where $\mathbf{U}^{(k)}$ is a 6×1 residual displacement vector. This yields five kinematic boundary conditions. For instance, the clamped boundary condition (that is, $\bar{\mathbf{u}}^{(k)} = \mathbf{0}\forall k$) can be realized as follows:

$$\tilde{\mathbf{v}}^{(1)} = \mathbf{0}, \quad \tilde{\mathbf{v}}^{(2)} = -\mathbf{H}_\theta^{-1} \langle \Theta^t \mathbf{N}_u \rangle \Gamma^{(1)} \mathbf{e}^{(1)}, \quad \dots, \quad \tilde{\mathbf{v}}^{(k)} = -\mathbf{H}_\theta^{-1} \langle \Theta^t \mathbf{N}_u \rangle (\bar{\mathbf{u}}_w^{(k)} + \bar{\mathbf{u}}_f^{(k)}), \quad k \geq 3, \quad (58)$$

where $\mathbf{H}_\theta \equiv \langle \Theta^t \Theta \rangle$. This however should be rearranged for each macroscopic problem so that

$$\hat{\mathbf{v}}^{(k)} = [\tilde{\mathbf{v}}_1^{(k)} \quad \tilde{\mathbf{v}}_2^{(k)} \quad \tilde{\mathbf{v}}_3^{(k-1)} \quad \tilde{\mathbf{v}}_4^{(k)} \quad \tilde{\mathbf{v}}_5^{(k)}]^t. \quad (59)$$

5. Numerical examples and discussion

Laminated and sandwich plates are considered as illustrative examples for the present asymptotic formulation. In order to investigate the edge effects, semiinfinite plates (that is, the 3D plane strain problem) with simply supported or clamped-free boundary conditions are analyzed (see Figure 2). The present results are compared to those obtained by 3D elasticity and Reissner–Mindlin plate theory, also known as first-order shear deformation theory (FSDT). The shear correction factor is assumed to be 5/6 for FSDT. For convenience, the present approach is referred to as a formal asymptotic method-based plate analysis (FAMPA) throughout the numerical examples.

The ply material properties of all the laminated plates are taken from [Pagano 1970], and are

$$E_L = 172.4 \text{ GPa}, \quad E_T = 6.9 \text{ GPa}, \quad G_{LT} = 3.45 \text{ GPa}, \quad G_{TT} = 1.38 \text{ GPa}, \quad \nu_{LT} = \nu_{TT} = 0.25, \quad (60)$$

where L denotes the direction of the fiber and T denotes the direction perpendicular to the fiber. For sandwich plates, the material properties of the face sheets are the same as those in (60), and the core material properties are given by

$$\begin{aligned} E_1 &= 0.1 \text{ GPa}, & G_{12} &= 0.04 \text{ GPa}, & \nu_{12} &= 0.25, \\ E_2 = E_3 &= E_1, & G_{23} = G_{13} &= G_{12}, & \nu_{23} = \nu_{13} &= \nu_{12}. \end{aligned} \quad (61)$$

Four cases including a sandwich plate are considered for two sets of boundary conditions, which are listed in Table 1. The elastic constants c_{ijkl} can be then calculated by using the moduli given in (60) and (61) and the fiber angle given in Table 1. Their explicit form can be found in [Reddy 2004].

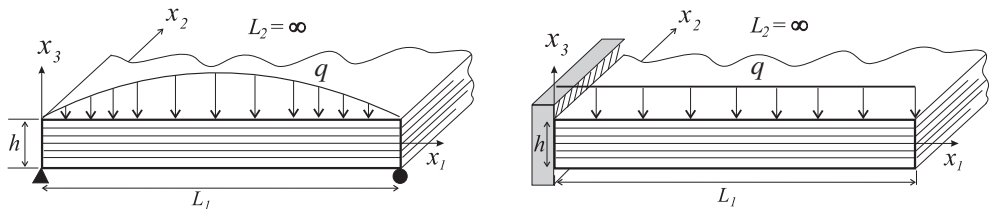


Figure 2. Loading and boundary conditions of semiinfinite plates: simply supported plate under sinusoidal pressure (left) and clamped-free plate under uniform pressure (right).

In all figures and tables, the k -th order solutions of the FAMPA are represented by

$$\mathbf{u}^{<k>} = \sum_{i=0}^k [\epsilon^{i+1} u_{\alpha}^{(i+1)} \quad \epsilon^i u_3^{(i)}]^t, \quad \boldsymbol{\sigma}^{<k>} = \sum_{i=1}^{k+1} \epsilon^i \boldsymbol{\sigma}^{(i)}, \quad k \geq 0, \quad (62)$$

so that the zeroth-order solution represents that of classical lamination theory (CLT) with $\sigma_{i3} = 0$ and the second-order solution represents that of the FSDT-like theory. Unlike in FSDT, the present second-order solution produces all the stress states including the transverse normal stress via the constitutive law. In the figures, the transverse stresses of the FSDT are calculated by using 3D equilibrium equations.

The displacement and stresses reported herein are normalized as follows [Pagano 1970]:

$$u_{\alpha}^* = 100E_T \frac{u_{\alpha}}{q_o} h S^3, \quad u_3^* = 100E_T \frac{u_3}{q_o} h S^4, \quad \sigma_{\alpha\beta}^* = \frac{\sigma_{\alpha\beta}}{q_o} S^2, \quad \sigma_{\alpha 3}^* = \frac{\sigma_{\alpha 3}}{q_o} S, \quad \sigma_{33}^* = \frac{\sigma_{33}}{q_o}, \quad (63)$$

where $S = L_1/h$ is the length-to-thickness ratio and q_o is the maximum of the applied pressure q .

5.1. Simply supported plates. For the problem of simply supported laminated and sandwich plates under sinusoidal pressure, the elasticity solution is available from [Pagano 1970], and has been used as the benchmark problem. In this case, problematic displacement prescribed boundary conditions are not involved. It is therefore possible to find the asymptotic solutions up to any desired order. For the purpose of comparison, the solutions of 3D elasticity and FSDT are also reproduced.

Case	Layup	x_3/h
1	[0.5 / 90.5 / 90.5 / 0.5]	{-1/2, -1/4, 0, 1/4, 1/2}
2	[90.5 / 0.5 / 90.5 / 0.5]	{-1/2, -1/4, 0, 1/4, 1/2}
3	[-30 / 30 / -30 / 30]	{-1/2, -1/4, 0, 1/4, 1/2}
4	[0.05 / Core / 0.05]	{-1/2, -2/5, 0, 2/5, 1/2}

Table 1. Lamination sequences for laminated and sandwich plates.

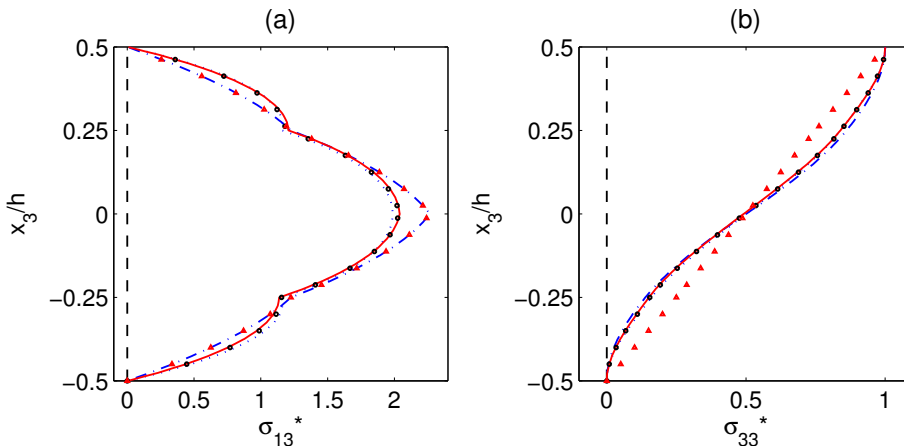


Figure 3. Transverse stresses of a simply supported plate, case 3, $S = 4$: σ_{13}^* (a) and σ_{33}^* (b). Exact (\bullet), FSDT (Δ), FAMPA 0th (—), FAMPA 2nd (— · —), FAMPA 4th (\cdots), and FAMPA 6th (—).

S	Models	Case 1	$\epsilon\%$	Case 2	$\epsilon\%$	Case 3	$\epsilon\%$	Case 4	$\epsilon\%$
4	Exact	3.3364	0	4.1812	0	3.2915	0	75.58	0
	FSDT	2.7299	-18	3.2964	-21	2.7868	-15	8.27	-89
	FAMPA 0th	0.5586	-83	1.1251	-73	0.9988	-70	1.01	-99
	FAMPA 2nd	3.5912	8	4.5380	9	3.4428	5	108.07	43
	FAMPA 4th	3.2689	-2	4.0805	-2	3.2655	-1	61.00	-19
	FAMPA 6th	3.3553	1	4.2121	1	3.2963	0	82.15	9
10	Exact	1.0359	0	1.6600	0	1.3854	0	17.01	0
	FSDT	0.9061	-13	1.4726	-11	1.2849	-7	2.17	-87
	FAMPA 0th	0.5586	-46	1.1251	-32	0.9988	-28	1.01	-94
	FAMPA 2nd	1.0438	1	1.6712	1	1.3899	0	18.14	7
	FAMPA 4th	1.0356	-0	1.6595	-0	1.3853	-0	16.93	-0
	20	Exact	0.6794	0	1.2609	0	1.0963	0	5.22
FSDT		0.6455	-5	1.2120	-4	1.0703	-2	1.30	-75
FAMPA 0th		0.5586	-18	1.1251	-11	0.9988	-9	1.01	-81
FAMPA 2nd		0.6799	0	1.2617	0	1.0966	0	5.29	1

Table 2. Comparison of center deflections of simply supported plates under sinusoidal loads.

Normalized center deflections of simply supported plates are listed and compared to the 3D elasticity solution in [Table 2](#). FSDT shows significant improvement compared to the FAMPA-0th or CLT for laminated plates, [cases 1–3](#). It however does not yield accurate predictions for the case of a sandwich plate. In fact, FSDT just produces comparable results to CLT even for $S \geq 20$. In contrast, the FAMPA-2nd results are practically identical to the 3D elasticity solution. Although the FAMPA-6th is necessary for accurate prediction in the case of very thick plates, $S = 4$, the FAMPA-2nd produces reasonable accuracy when $S \geq 10$ for both laminated and sandwich plates. Local through-the-thickness distributions of stresses are also important in analysis of composite plates. Transverse stresses for an antisymmetric laminated plate are presented in [Figure 3](#) and those for a sandwich plate in [Figure 4](#). It is seen that the FAMPA asymptotically converges to the 3D elasticity with increasing ϵ -order level. The transverse shear stress of the FAMPA-2nd is identical to that of FSDT, whereas the transverse normal stress of FSDT significantly deviates from the FAMPA-2nd and the 3D elasticity, which is clearly shown in [Figure 4b](#).

5.2. Clamped-free plates. We now consider clamped-free plates, investigating displacement-prescribed and traction-free boundary conditions. Unlike the simply supported plate with sinusoidal loadings, our analysis is restricted to the FAMPA-2nd because the asymptotically correct displacement boundary condition is only available up to the second order, which is given in [\(59\)](#). In addition, there is difficulty in calculating higher-order derivatives with respect to y_α in the framework of a finite element method.

Normalized tip deflections of clamped-free laminated and sandwich plates with a function of the length-to-thickness ratio S are shown in [Figure 5](#) for [cases 3 and 4](#). The FAMPA-2nd performs similarly to FSDT for [case 3](#). For a sandwich plate, FSDT significantly deviates from the 3D FEM, whereas the FAMPA-2nd is very close to it. This clearly indicates that it is of great importance to apply a proper

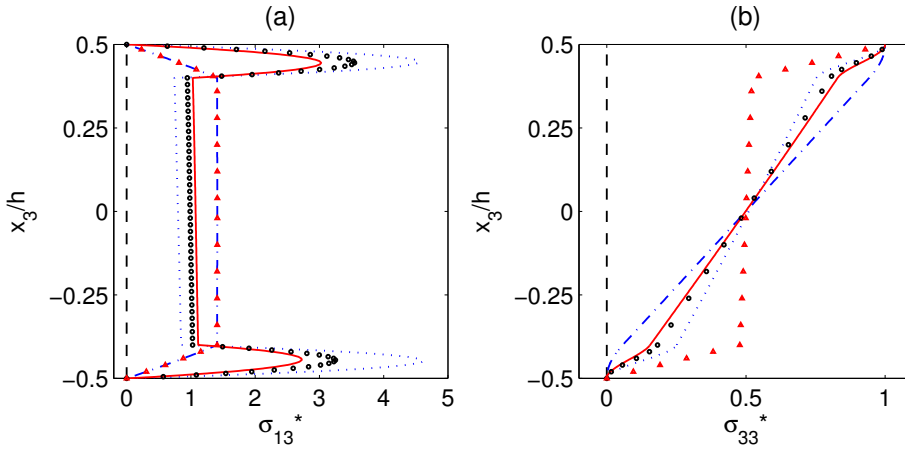


Figure 4. Transverse stresses of a simply supported plate, case 4, $S = 4$: σ_{13}^* (a) and σ_{33}^* (b). Exact (\bullet), FSDT (Δ), FAMPA 0th (—), FAMPA 2nd (— · —), FAMPA 4th (\cdots), and FAMPA 6th (—).

set of edge boundary conditions especially for a plate weak in shear. To more clearly demonstrate this, the bending deflection and slope along the normalized in-plane coordinate are illustrated in Figure 6 for a sandwich plate with $S = 10$. The error of the FSDT is more than 400% in terms of tip deflection, whereas the FAMPA-2nd shows reasonable accuracy. This is achieved by improving a clamped boundary condition in which the bending slope is not zero, as shown in Figure 6b, where the interior solution is approximately valid for 30% to 80% from the clamped end. Local stress distributions are also investigated, and stresses of a thick antisymmetric cross-ply plate at the midspan of the plate are illustrated in Figure 7. The transverse shear stress of the FAMPA-2nd coincides with that of FSDT, since σ_{13} is calculated by using the 3D equilibrium equation for FSDT. In-plane and transverse normal stresses calculated by the

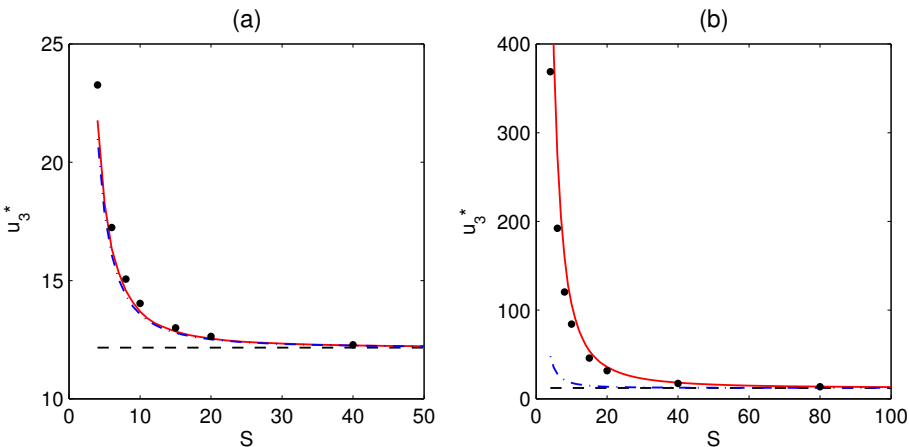


Figure 5. Tip deflections of clamped-free laminated and sandwich plates: antisymmetric angle-ply (a), case 3, and sandwich (b), case 4. 3D FEM (\bullet), FSDT (— · —), FAMPA 0th (—), and FAMPA 2nd (—).

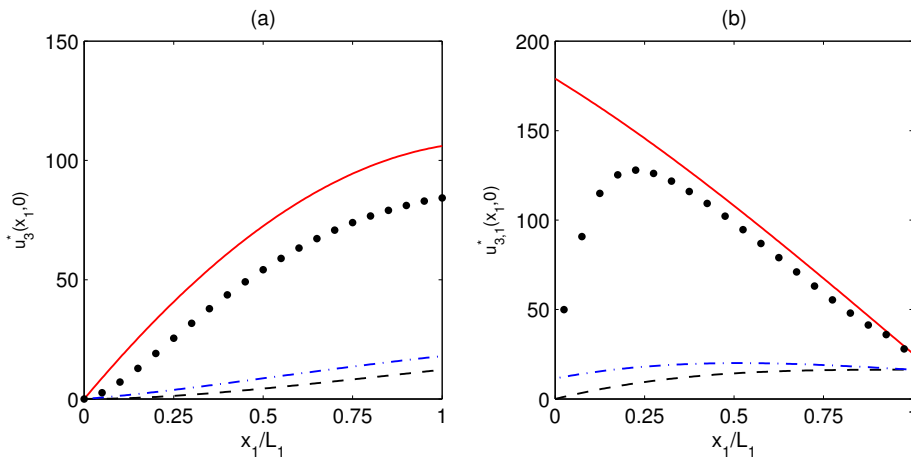


Figure 6. A clamped-free sandwich plate, **case 4**, $S = 10$: bending deflection (a), and bending slope (b). 3D FEM (\bullet), FSDT ($- \cdot -$), FAMPA 0th ($--$), and FAMPA 2nd ($-$).

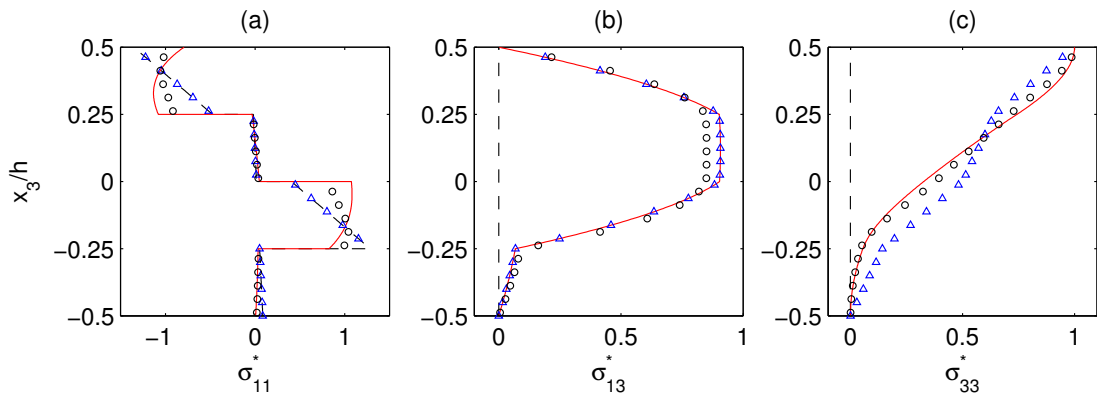


Figure 7. Stresses of a clamped-free antisymmetric cross-ply laminated plate, **case 2**, $S = 4$: σ_{11}^* (a), σ_{13}^* (b), and σ_{33}^* (c). 3D FEM (\circ), FSDT (Δ), FAMPA 0th ($--$), and FAMPA 2nd ($-$).

FAMPA-2nd are well correlated with the 3D FEM, whereas FSDT yields erroneous results qualitatively as well as quantitatively.

To investigate the edge layer effects, the in-plane normal stresses calculated at near the clamped-end, midspan, and near the free-end, which are located at the 12%, 49%, and 87% axial positions from the clamped end, respectively, are plotted in **Figure 8** for a thick symmetric cross-ply plate. The best approximation of the FAMPA-2nd to the 3D FEM can be seen in the midspan where the interior solution is valid. Near the clamped end, the FAMPA-2nd tends to produce a through-the-thickness stress distribution similar to that in the interior region because we applied the asymptotically correct boundary condition up to the second order only. It can however accurately capture the stress-free edge layer effect, as shown in **Figure 8c** where the FAMPA-2nd drastically improves the prediction of the in-plane stress compared

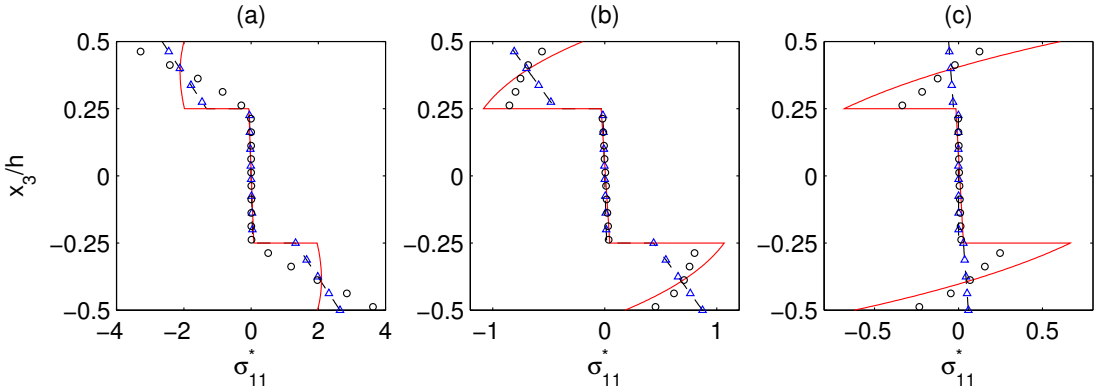


Figure 8. In-plane normal stress of a clamped-free symmetric cross-ply laminated plate, **case 1**, $S = 4$: near the clamped-end (a), midspan (b), and near the free-end (c). 3D FEM (\circ), FSDT (Δ), FAMPA 0th (— —), and FAMPA 2nd (—).

to FSDT and the FAMPA-0th. It is of interest that the in-plane normal stress is not that small even if the in-plane stress is zero at the free-end.

5.3. Usefulness of the FAMPA. Through-the-thickness warping functions are discussed in this subsection. An antisymmetric angle-ply laminated plate, **case 3**, is considered as an example. The proposed asymptotic analysis method may be limited to second-order analysis because higher-order analysis requires both higher-order asymptotically correct displacement boundary conditions as well as higher-order derivatives. The requirement of higher-order derivatives of the macroscopic strain measure $\mathbf{e}^{(k)}$ makes it difficult to realize the FAMPA with a finite element method. Although the FAMPA-2nd yields reasonable accuracy for most engineering applications, one may want to look at higher-order effects. In this case, the warping functions $\Gamma_{\alpha\beta\dots\psi\omega}^{(k)}$ can provide useful information without solving the macroscopic problems.

The first-order through-the-thickness deformation mode of **case 3** is shown in **Figure 9**. This mode mainly illustrates the 3D Poisson effect that represents the deformation along the thickness direction. **Figure 9** implies that the out-of-plane displacements consist of linear and quadratic variations, in which the linear variation accounts for the in-plane tension induced deformation and the quadratic variation explains the bending induced deformation. In general these variations are smeared into the reduced stiffness models that are often derived by applying the plane stress assumption of $\sigma_{33} = 0$. The first nonclassical through-the-thickness mode, such as a transverse shear deformation effect, can be found in $\Gamma_{\alpha}^{(2)}$. For example, $\Gamma_1^{(2)}$ are plotted in **Figures 10** and **11**. Unlike the first deformation mode $\Gamma^{(1)}$, the in-plane displacements u_{α} play a major role in this mode. **Figure 10** depicts the displacement component u_1 , which clearly shows a transverse shear deformation effect due to the bending deformations corresponding to $\kappa_{11,1}$ and $\kappa_{22,1}$. The contribution of $\kappa_{22,1}$ to u_1 is obvious because of the antisymmetric configuration. For this reason, the higher-order bending curvature $\kappa_{11,1}$ also contributes to the displacement component u_2 as shown in **Figure 11**. The through-the-thickness warping functions presented in **Figure 11** have a unique pattern depending on the lamination configurations, which could be very difficult to presuppose.

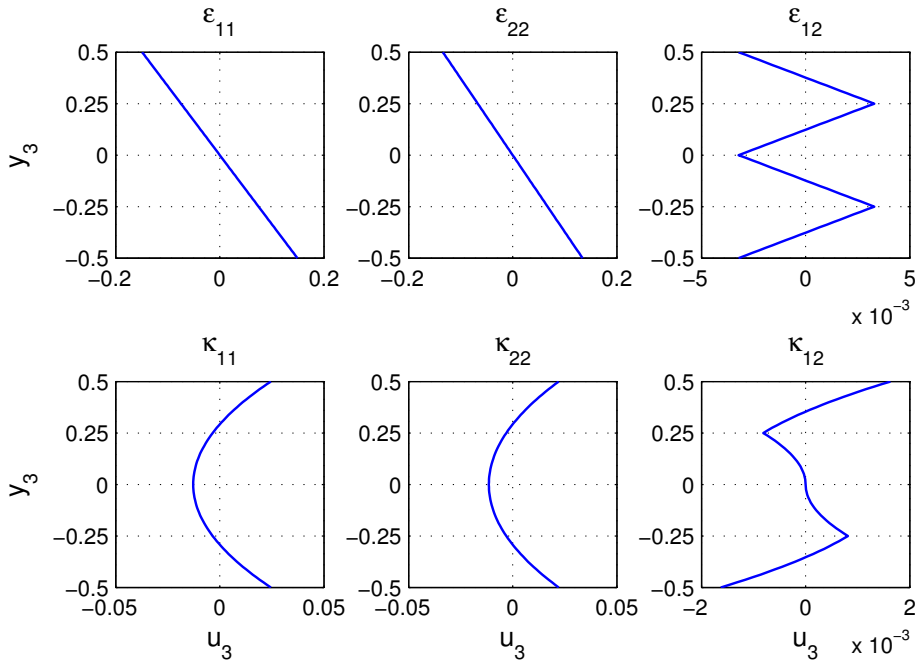


Figure 9. The first-order through-the-thickness deformation mode (u_3) of an antisymmetric angle-ply laminated plate, case 3, $\Gamma^{(1)}$.

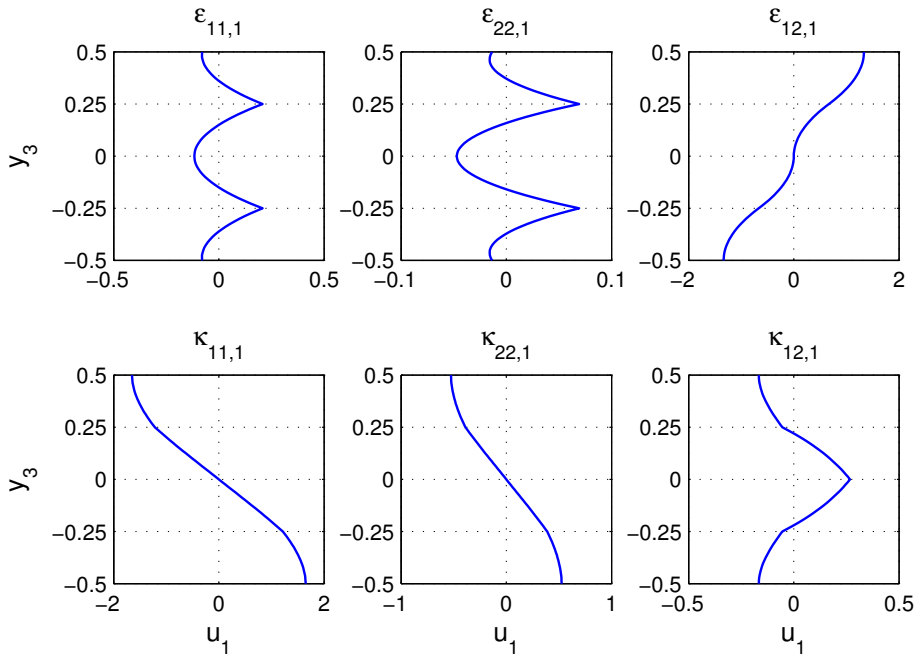


Figure 10. The second-order through-the-thickness deformation mode (u_1) of an antisymmetric angle-ply laminated plate, case 3, $\Gamma_1^{(2)}$.

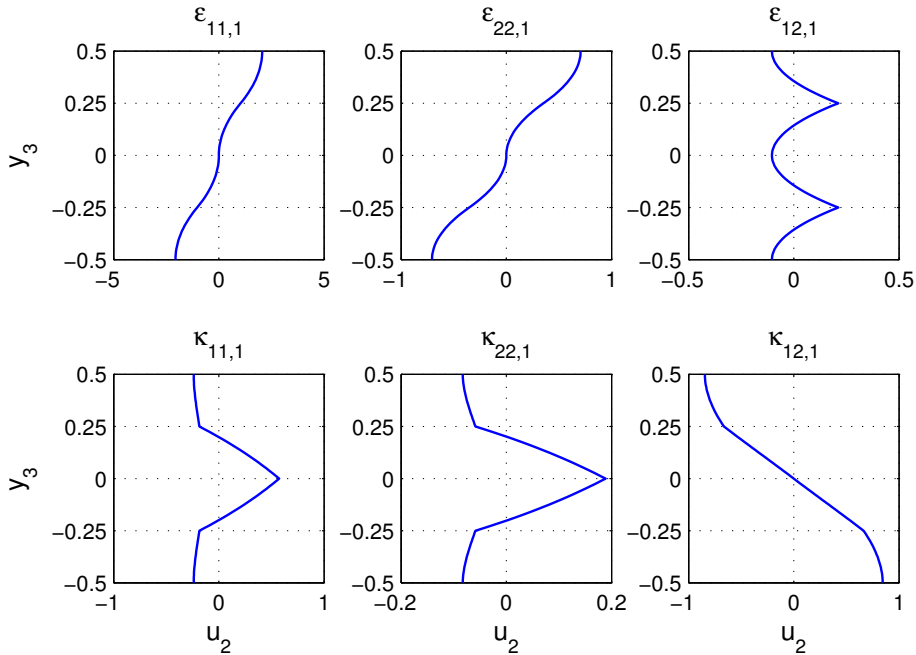


Figure 11. The second-order through-the-thickness deformation mode (u_2) of an anti-symmetric angle-ply laminated plate, case 3, $\Gamma_1^{(2)}$.

6. Conclusions

A formal asymptotic method-based plate analysis (FAMPA) is developed to analyze general anisotropic plates. To assess the FAMPA capability for various sets of boundary conditions, simply supported and clamped-free boundary conditions are considered. For a simply supported boundary condition, it is demonstrated that the FAMPA can provide the exact solutions by increasing the order up to the sixth order for very thick plates. The orthogonality condition of asymptotic displacements to the fundamental solution is adopted to avoid the complexity of using the decay analysis method for a displacement prescribed boundary. The boundary conditions obtained, which are asymptotically correct up to the second order, are applied to plates with clamped-free boundary conditions. The results are compared to those of the three-dimensional FEM and FSDT. It is demonstrated that the FAMPA-2nd is simple enough for engineering applications and accurate enough for high precision analysis. It can also simulate the free-edge boundary layer effect qualitatively, whereas FSDT cannot. Although a higher-order computation of the FAMPA is practically limited due to the displacement boundary conditions and the higher order derivatives of the macroscopic strain measure, one can have in-depth understanding of the higher-order behaviors of such composite plates via the microscopic analysis up to any desired order. The through-the-thickness warping functions obtained can be also used for development and validation of any higher-order plate theories.

References

- [Berdichevskii 1979] V. L. Berdichevskii, “Variational-asymptotic method of constructing a theory of shells”, *J. Appl. Math. Mech.* **43**:4 (1979), 711–736.

- [Berg 1991] L. J. Berg, “Asymptotic variational methods in large deflection small strain plate theory”, *Int. J. Solids Struct.* **27**:11 (1991), 1401–1417.
- [Buannic and Cartraud 2001] N. Buannic and P. Cartraud, “Higher-order effective modeling of periodic heterogeneous beams, I: Asymptotic expansion method”, *Int. J. Solids Struct.* **38**:40–41 (2001), 7139–7161.
- [Carrera 2003] E. Carrera, “Historical review of Zig-Zag theories for multilayered plates and shells”, *Appl. Mech. Rev. (ASME)* **56**:3 (2003), 287–308.
- [Cesnik et al. 1996] C. E. S. Cesnik, V. G. Sutyryn, and D. H. Hodges, “Refined theory of composite beams: the role of short-wavelength extrapolation”, *Int. J. Solids Struct.* **33**:10 (1996), 1387–1408.
- [Duva and Simmonds 1992] J. M. Duva and J. G. Simmonds, “The influence of two-dimensional end effects on the natural frequencies of cantilevered beams weak in shear”, *J. Appl. Mech. (ASME)* **59**:1 (1992), 230–232.
- [Fan and Widera 1994] H. Fan and G. E. O. Widera, “On the use of variational principles to derive beam boundary conditions”, *J. Appl. Mech. (ASME)* **61**:2 (1994), 470–471.
- [Gregory and Wan 1984] R. D. Gregory and F. Y. M. Wan, “Decaying states of plane strain in a semi-infinite strip and boundary conditions for plate theory”, *J. Elasticity* **14**:1 (1984), 27–64.
- [Horgan and Simmonds 1991] C. O. Horgan and J. G. Simmonds, “Asymptotic analysis of an end-loaded, transversely isotropic, elastic, semi-infinite strip weak in shear”, *Int. J. Solids Struct.* **27**:15 (1991), 1895–1914.
- [Kapania and Raciti 1989] R. K. Kapania and S. Raciti, “Recent advances in analysis of laminated beams and plates, I: shear-effects and buckling”, *AIAA J.* **27**:7 (1989), 923–935.
- [Kim et al. 2008] J.-S. Kim, M. Cho, and E. C. Smith, “An asymptotic analysis of composite beams with kinematically corrected end effects”, *Int. J. Solids Struct.* **45**:7–8 (2008), 1954–1977.
- [Lo et al. 1977] K. H. Lo, R. M. Christensen, and F. M. Wu, “A higher-order theory of plate deformation, II: Laminated plates”, *J. Appl. Mech. (ASME)* **44** (1977), 669–676.
- [Niordson 1979] F. I. Niordson, “An asymptotic theory for vibrating plates”, *Int. J. Solids Struct.* **15**:2 (1979), 167–181.
- [Noor and Burton 1989] A. K. Noor and W. S. Burton, “Assessment of shear deformation theories for multilayered composite plates”, *Appl. Mech. Rev. (ASME)* **42** (1989), 1–13.
- [Novotny 1970] B. Novotny, “On the asymptotic integration of the three-dimensional non-linear equations of thin elastic shells and plates”, *Int. J. Solids Struct.* **6**:4 (1970), 433–451.
- [Pagano 1970] N. J. Pagano, “Influence of shear coupling in cylindrical. Bending of anisotropic laminates”, *J. Compos. Mater.* **4**:3 (1970), 330–343.
- [Reddy 2004] J. N. Reddy, *Mechanics of laminated composite plates and shells: theory and analysis*, 2nd ed., CRC Press, Boca Raton, FL, 2004.
- [Reddy and Jr. 1994] J. N. Reddy and D. H. R. Jr., “Theories and computational models for composite laminates”, *Appl. Mech. Rev. (ASME)* **47** (1994), 147–169.
- [Tarn et al. 1996] J.-Q. Tarn, Y.-B. Wang, and Y.-M. Wang, “Three-dimensional asymptotic finite element method for anisotropic inhomogeneous and laminated plates”, *Int. J. Solids Struct.* **33**:13 (1996), 1939–1960.
- [Wang and Tarn 1994] Y.-M. Wang and J.-Q. Tarn, “A three-dimensional analysis of anisotropic inhomogeneous and laminated plates”, *Int. J. Solids Struct.* **31**:4 (1994), 497–515.
- [Yu 2005] W. Yu, “Mathematical construction of a Reissner-Mindlin plate theory for composite laminates”, *Int. J. Solids Struct.* **42**:26 (2005), 6680–6699.
- [Yu et al. 2002] W. Yu, D. H. Hodges, and V. V. Volovoi, “Asymptotic construction of Reissner-like composite plate theory with accurate strain recovery”, *Int. J. Solids Struct.* **39**:20 (2002), 5185–5203.

Received 23 Nov 2008. Revised 5 Mar 2009. Accepted 18 Mar 2009.

JUN-SIK KIM: junsik.kim@kumoh.ac.kr

School of Mechanical Engineering, Kumoh National Institute of Technology, Gumi, Gyeongbuk 730-701, Korea